Chin. J. Mech. Eng. (2017) 30:1296–1304
https://doi.org/10.1007/s10033-017-0192-3

ORIGINAL ARTICLE

An Intelligent Harmonic Synthesis Technique for Air-Gap Eccentricity Fault Diagnosis in Induction Motors

De Z. Li[1] · Wilson Wang[1] · Fathy Ismail[2]

Received: 15 June 2017 / Revised: 28 August 2017 / Accepted: 29 September 2017 / Published online: 21 November 2017

Abstract Induction motors (IMs) are commonly used in various industrial applications. To improve energy consumption efficiency, a reliable IM health condition monitoring system is very useful to detect IM fault at its earliest stage to prevent operation degradation, and malfunction of IMs. An intelligent harmonic synthesis technique is proposed in this work to conduct incipient air-gap eccentricity fault detection in IMs. The fault harmonic series are synthesized to enhance fault features. Fault related local spectra are processed to derive fault indicators for IM air-gap eccentricity diagnosis. The effectiveness of the proposed harmonic synthesis technique is examined experimentally by IMs with static air-gap eccentricity and dynamic air-gap eccentricity states under different load conditions. Test results show that the developed harmonic synthesis technique can extract fault features effectively for initial IM air-gap eccentricity fault detection.

Keywords Air-gap eccentricity · Current signal · Fault detection · Induction motor

Supported in part by Natural Sciences and Engineering Research Council of Canada (NSERC), eMech Systems Inc and Bare Point Water Treatment Plant in Thunder Bay, Ontario, Canada.

✉ Wilson Wang
wwang3@lakeheadu.ca

[1] Department of Mechanical Engineering, Lakehead University, Thunder Bay, ON P7B 7C1, Canada

[2] Department of Mechanical & Mechatronics Engineering, University of Waterloo, Waterloo, ON N2L 3G1, Canada

1 Introduction

Induction motors (IMs) are commonly used in various industrial applications. Furthermore, IMs consume about 50% of the generated electrical energy in the world [1]. IM defects will lead to low productivity and inefficient energy consumption. Endeavors have been put, for decades, to improve IM operation accuracy and IM driven industrial process efficiency. In industrial maintenance applications, for example, an efficient and reliable IM condition monitor is very useful to detect an IM defect at its earliest stage to prevent malfunction of IMs and reduce maintenance cost.

In general, air-gap eccentricity is classified as static eccentricity, dynamic eccentricity, as well as mixed eccentricity of these two types [2]. In static air-gap eccentricity, geometric axis of rotor rotation is not the geometric axis of the stator, and position of the minimal radial air-gap length is fixed in space. In dynamic air-gap eccentricity, the rotor rotates around the geometric axis of the stator, where the position of the minimum air-gap length rotates with the rotor. In a particular case of static air-gap eccentricity, rotor geometric axis is not parallel to stator geometric axis; the degree of eccentricity gradually changes along stator axis, which is inclined static eccentricity [3]. IM air-gap eccentricity defects could result in unbalanced magnetic pull, bearing damage, excessive vibration and noise, and even stator-rotor rub failure [4]. Correspondingly, this work will focus on initial IM fault detection of static eccentricity and dynamic eccentricity.

Recently, many research efforts have been undertaken to diagnose IM air-gap eccentricity fault using stator current signals due to their low cost and ease of implementation [5, 6]. For example, Blödt et al. [7] presented a Wigner distribution method to analyze stator current signals and diagnose IM eccentricity fault. Akin et al. [8] conducted

real-time eccentricity fault detection using reference frame theory. Bossio et al. [9] employed additional excitation to reveal information about air-gap eccentricity fault. Alarcon et al. [10] applied notch finite-impulse response filter and Wigner-Ville Distribution to study rotor asymmetries and mixed eccentricities. Faiz et al. [11] employed instantaneous power harmonics to detect mixed IM eccentricity defect. Huang et al. [12] applied an artificial neural network for the detection of rotor eccentricity faults. Esfahani et al. [13] utilized the Hilbert-Huang transform to detect IM eccentricity fault. Nandi et al. [14] studied the eccentricity fault related harmonics with different rotor cages. Riera-Guasp et al. [15] applied Gabor analysis for transient current signals to detect eccentricity fault. Park and Hur [16] analyzed specific frequency patterns of the stator current to detect dynamic eccentricity fault. Mirimani et al. [17] presented an online diagnostic method for static eccentricity fault detection. Some intelligent tools based on soft computing and pattern classification were also used for motor fault diagnosis in Refs. [18–20], in order to explore patterns of the features. These aforementioned techniques, however, cannot thoroughly explore the relations among massive fault harmonic series in the current spectrum, which may degrade fault detection accuracy.

To tackle the aforementioned problems with IM fault detection using current signals, a harmonic synthesis (HS) technique is proposed in this work for incipient IM eccentricity fault detection. The contributions of the proposed HS technique lie in the following aspects: 1) a novel synthesis approach is proposed to integrate several fault harmonic series to recognize fault related features; 2) fault indicators are properly derived from local spectra for IM health condition monitoring. The effectiveness of the proposed HS technique for IM eccentricity defect detection is verified experimentally under different IM conditions.

The remainder of this paper is organized as follows. The proposed HS technique is discussed in Section 2. Effectiveness of the HS technique for IM air-gap eccentricity fault detection is examined experimentally in Section 3. Finally, some concluding remarks of this study are summarized in Section 4.

2 The Proposed HS Technique for IM Eccentricity Fault Detection

The proposed HS technique is composed of two procedures: harmonic series processing (HSP) and local spectra analysis (LSA). The HSP is to synthesize the fault related features in the spectrum, whereas LSA is to extract fault indicators for incipient IM air-gap eccentricity fault detection.

2.1 Harmonic Series Processing

In stator current signal based IM fault detection, the characteristic frequency components f_e in Hz used to detect static and dynamic eccentricity defects [21] are given by

$$f_e = f_s\left[(kR \pm \alpha)\frac{1-s}{p} \pm \beta\right] = (kR \pm \alpha)f_r \pm \beta f_s \tag{1}$$

where f_s is the supply frequency in Hz; R is the number of rotor slots; s is the slip; f_r is the rotor rotating speed; $k = 1, 2, 3, \ldots$; p is the number of pole pairs; $\beta = 1, 3, 5, \ldots$ is the order of the stator time harmonics; α is the eccentricity order: $\alpha = 0$ denotes static eccentricity and $\alpha = 1$ denotes dynamic eccentricity.

The Kth order fault harmonic series f_{e_K} will be

$$f_{e\_K} = f_{o\_K} + \beta f_s, \quad \beta = 1, 3, 5, \ldots \tag{2}$$

where the Kth order origin frequency component f_{o_K} is

$$f_{o\_K} = (kR \pm \alpha)f_r \tag{3}$$

To explore the relationship among different fault harmonic series, the fault harmonic series of interest are synthesized to reveal fault characteristic features. If the first P fault harmonics ($\beta = 1, 3, 5, \ldots, 2P–1$) are considered for synthesis, the harmonic frequency band corresponding to the Kth fault harmonic series will be extracted as

$$q_K = [f_{o\_K}, f_{o\_K} + 2Pf_s] \tag{4}$$

and the bandwidth in Hz is $2Pf_s + 1$.

To synthesize fault harmonic series, the frequency bands are converted to a discrete-point domain representation. The discrete-point closest to f_{o_K} is considered as the first discrete-point in q_K, defined as $D_k\{1\}$. Suppose u_f discrete data points represent unit frequency distance in the spectrum, the bandwidth of Eq. (4) in discrete-point domain will be formulated as

$$B_w = \langle 2Pf_s + 1\rangle u_f \tag{5}$$

where $\langle\cdot\rangle$ denotes the integer function. Then the harmonic frequency band of Eq. (4) in the discrete-point domain will be

$$D_K\{i\}, \quad i = 1, 2, 3, \ldots, B_w \tag{6}$$

The root-mean-square (RMS) operation is applied to synthesize harmonic frequency bands. Given the harmonic frequency bands of M interested fault harmonic series, the ith component in the synthesized spectrum v will be derived as

$$v\{i\} = \sqrt{\frac{\sum_{j=1}^{M} D_j\{i\}^2}{M}} \quad i = 1, 2, 3, \ldots, B_w \tag{7}$$

2.2 Local Spectra Analysis

The mth harmonic ($\beta = 2\ m–1$) of the Kth order fault harmonic series will be derived from Eq. (2),

$$f_{K,m} = f_{o\_K} + (2m-1)f_s \tag{8}$$

Through the synthesis operation in Eq. (7), the mth fault harmonic over all M harmonic frequency bands is synthesized to form a new fault frequency component. Then the mth synthesized fault frequency component in the discrete-point domain will be derived in the synthesized spectrum by the following representation:

$$v\{1 + (2m-1)f_s u_f\} \tag{9}$$

The local spectra encompassing the mth synthesized fault frequency component will be

$$\left[v\{1 + (2m-1)f_s u_f - du_f\},\ v\{1 + (2m-1)f_s u_f + du_f\}\right] \tag{10}$$

where d is the half bandwidth of the local spectra in the frequency domain. The mean value of this local spectrum is the fault indicator regarding the mth synthesized fault frequency component, denoted by F_m.

To illustrate the operation of the proposed HSP and LSA processes, a simulated current spectrum with three air-gap eccentricity frequency harmonic series is illustrated in Figure 1. It is normalized by deducting mean and then being divided by its standard deviation. In Figure 1, the black arrow points 50 Hz supply frequency; magenta arrows with number 1, green arrows with number 2 and yellow arrows with number 3 denote three fault harmonic series respectively. The origin frequency components f_{o_K} are 114.1 Hz, 142.4 Hz, and 170.7 Hz, respectively. The harmonics of defect features are computed using Eq. (2) with $f_s = 50$ Hz and $\beta = 1, 3, 5, 7, 9$. Figure 1 shows that some fault characteristic frequency components are buried in the spectrum, and it is difficult to predict which characteristic frequency components will protrude in the spectrum. The extracted frequency bands represented in Eq. (6) of three fault harmonic series, and synthesized spectrum represented in Eq. (7) with fault related local spectra are demonstrated in Figure 2. The dashed vertical lines indicate the boundaries of local spectra encompassing synthesized fault frequency components. Figures 2(a), 2(b) and 2(c) represent three frequency bands computed by Eq. (4) with staring frequencies f_{o_K} being 114.1 Hz, 142.4 Hz, and 170.7 Hz, respectively. Figure 2(d) shows results of the synchronization of spectra in Figures 2(a), 2(b) and 2(c) using root-mean-square calculation using Eq. (7). It is seen from Figure 2(d) that the fault characteristic features can be highlighted in the spectrum after the HSP operation, which could be used for IM fault detection. In this simulation, the supply frequency $f_s = 50$ Hz; f_{o_K} is the starting point of the spectrum in Figure 2(d). Based on Eqs. (2) and (3), the fault frequencies in Figure 2(d) should appear at 50 Hz, 150 Hz, 250 Hz, 350 Hz and 450 Hz. The frequency components outside the boundaries of local spectra are usually caused by the modulation of load variation and supply frequency, and the synchronization of different harmonic series local bands.

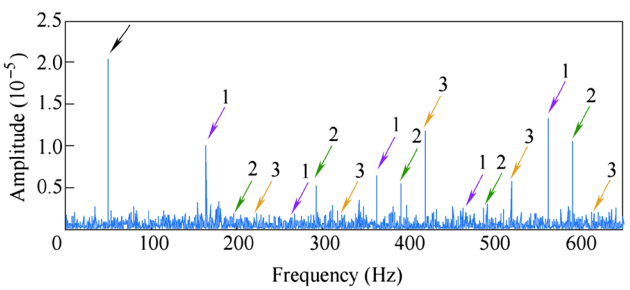

Figure 1 Simulated current spectrum with three air-gap eccentricity characteristic harmonic series

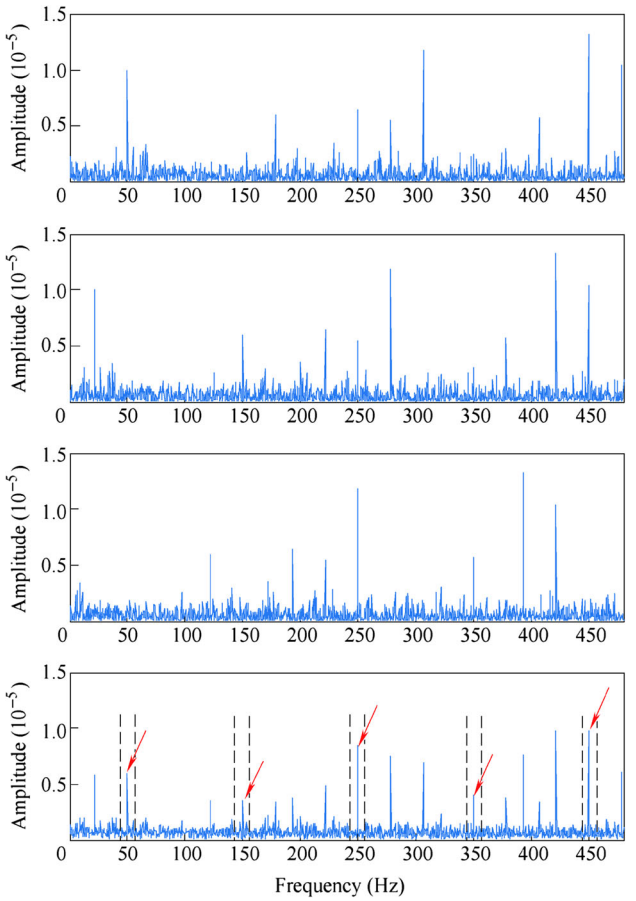

Figure 2 The frequency bands: (a) the magenta-arrowed harmonic series; (b) the green-arrowed harmonic series; (c) the yellow-arrowed harmonic series; (d) the synthesized spectrum of the frequency bands in (a), (b), and (c)

If both static and dynamic eccentricities occur simultaneously, the following characteristic frequency components could also be excited [22], given by

$$f'_e = |kf_r \pm f_s|, \quad k = 1, 2, 3, \ldots \tag{11}$$

The related harmonic series can be expressed as

$$f'_{e1} = kf_r + f_s, \quad k = 1, 2, 3, \ldots \tag{12}$$

$$f'_{e2} = kf_r - f_s, \quad k = 2, 3, \ldots \tag{13}$$

The local spectra of the first Q harmonics in Eq. (12) will be transformed to the discrete-point domain, and then synthesized into one spectrum in RMS form using Eq. (7). The mean value of the synthesized spectrum is considered as a fault indicator denoted by F_{d1}. The fault indicator derived from Eq. (13) will be denoted by F_{d2}.

3 Performance Evaluations

3.1 Overview

To examine the effectiveness of the proposed HS technique, a series of tests will be conducted for IM air-gap eccentricity fault diagnosis using stator current signals. This work focuses on both static and dynamic eccentricity fault detection. The parameters of the proposed HS technique used in the following tests are given in Table 1. To thoroughly analyze fault information, the first 20 fault harmonic series (i.e., $M = 5$) are synthesized and the first eight harmonics ($P = 8$) in the synthesized spectrum are utilized to generate fault indicators F_m, $m = 1, 2, \ldots, 8$. The frequency band [0, 8000] Hz is used for analysis. To analyze more informative fault features in harmonic series in Eqs. (12) and (13), the first ten harmonics are used to derive fault indicators F_{d1} and F_{d2}. To capture the fault features and exclude the interference nearby, the half bandwidth of the local spectra is selected as 2 Hz.

To derive F_m for eccentricity fault detection, the coefficient $\alpha = 0$ in Eq. (3) is set for static eccentricity detection and $\alpha = 1$ for dynamic eccentricity analysis. To evaluate the effectiveness of the HS technique, the power spectral density (PSD) is used for comparison. To implement PSD, the mean values of ten local bands are used as fault indicators, whose half bandwidth is set as 2 Hz. Eight of ten center frequencies of the local bands are calculated using Eq. (1) with $k = 1$ and $\beta = 1, 2, \ldots, 8$. The other two center frequencies are computed using f'_{e1} with $k = 1$ and

Table 1 Factors and their levels

f_s/Hz	P	u_f	Q	M	d/Hz
50	8	3	10	5	2

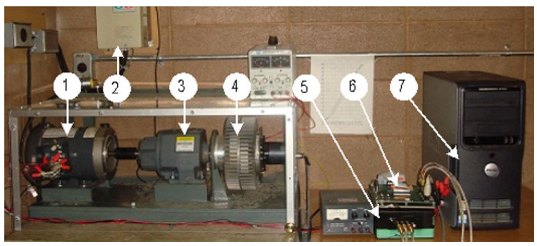

Figure 3 IM experiment setup. 1. Tested IM; 2. Speed controller; 3. Gearbox; 4. Load system; 5. Current sensors; 6. Data acquisition system; 7. Computer

Table 2 Motor specifications

Phase	Poles	HP	Connection	Rotor bars	Stator slots
3	2	1/3	Y	34	24

Table 3 Averaged successful rates (SR) of ten runs three-fold cross validation in terms of static air-gap eccentricity fault diagnosis using SVM (%)

Load level	0	20	50	70	100
PSD training SR	69.71	65.84	68.23	65.38	60.46
PSD test SR	65.97	61.49	65.52	61.66	53.57
HHT training SR	99.26	72.30	53.20	52.20	77.27
HHT test SR	98.41	71.59	48.76	51.20	74.99
CHS training SR	96.18	81.47	96.68	96.14	96.17
CHS test SR	94.54	78.92	95.79	94.73	95.77
HS training SR	100	100	99.56	100	97.87
HS test SR	100	100	99.20	100	97.28

Table 4 Averaged successful rates (SR) of ten runs three-fold cross validation in terms of static air-gap eccentricity fault diagnosis using LDA (%)

Load level	0	20	50	70	100
PSD training SR	73.09	69.41	68.37	71.07	68.47
PSD test SR	71.63	67.95	66.60	69.88	66.32
HHT training SR	93.13	72.94	66.87	67.92	77.96
HHT test SR	92.42	71.62	66.05	66.50	77.15
CHS training SR	95.98	80.79	96.69	94.47	93.57
CHS test SR	95.78	79.05	95.90	93.97	92.83
HS training SR	99.99	100	99.41	100	95.73
HS test SR	99.83	100	99.10	100	95.17

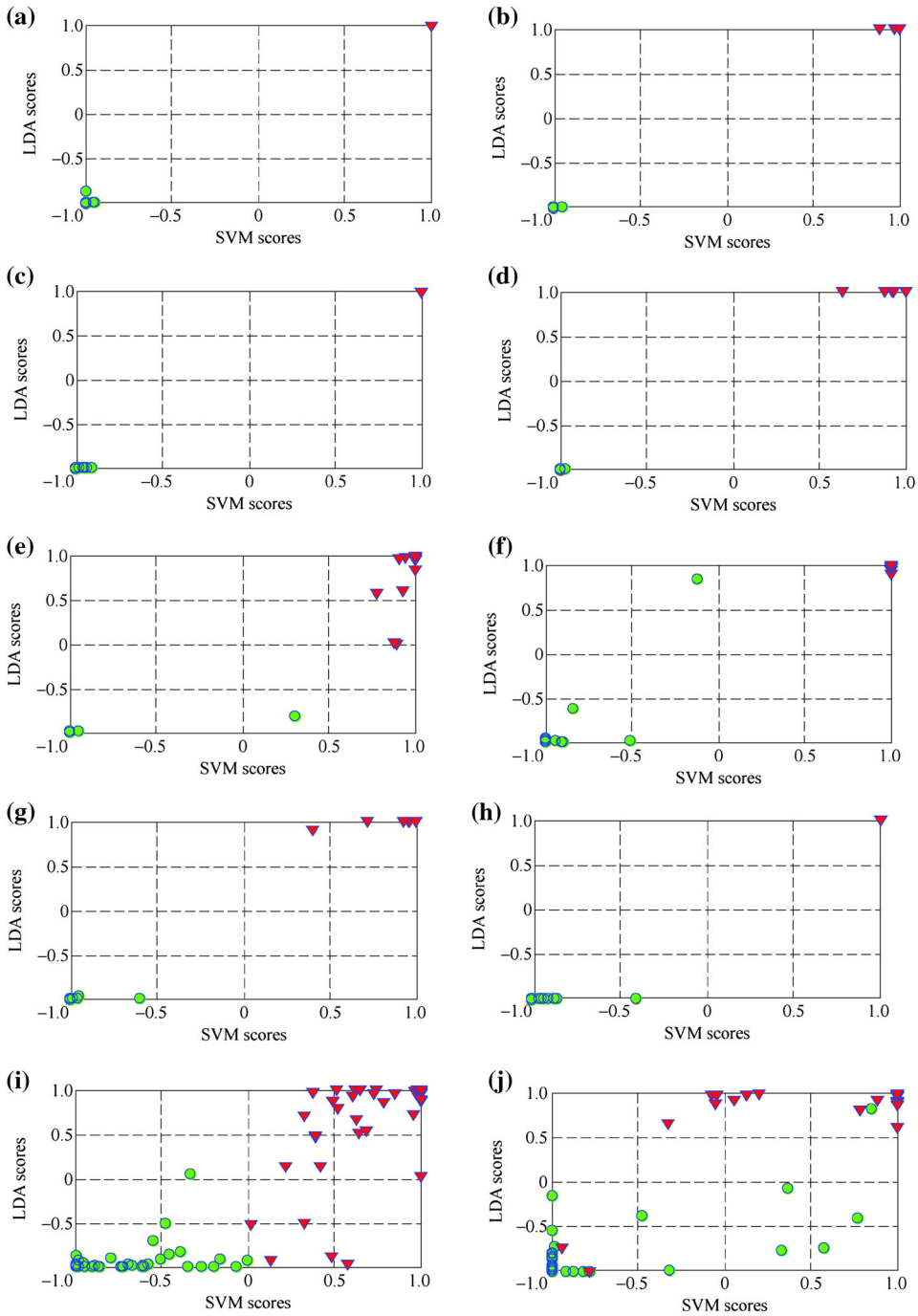

Figure 4 The score plots of SVM and LDA with respect to the HS static eccentricity fault indicators for static eccentricity diagnosis. The training data score distribution with different load conditions: (a) 0%, (c) 20%, (e) 50%, (g) 70% and (i) 100%, and test data score distribution in different conditions: (b) 0%, (d) 20%, (f) 50%, (h) 70% and (j) 100% load conditions. The green circles and the red triangles represent two different class samples respectively

f'_{e2} with $k = 2$. In addition, a variant of the HS technique is employed for comparison, in which the center characteristic frequencies in the synthesized local spectra rather than the mean values are utilized as fault indicators, and is denoted by CHS. The frequency components in Eq. (9) with $m = 1, 2, \ldots, 8$, and the two center frequencies of the synthesized local spectra derived from Eqs. (12) and (13), respectively, are used as fault indicators of the CHS method. The Hilbert-Huang transform (HHT) based fault indicators [13] will be used for comparison. Since this work focuses on the analysis of the current signal based fault indicators, only the current signal related fault indicators provided in Ref. [13] will be used for comparison. The HHT is applied to current signal analysis to generate fault indicators. The mean values of four local bands centered at f'_{e1} with $k = 1, 2$, and f'_{e2} with $k = 2, 3$, and averaged Hilbert marginal spectrum in local bands centered at f'_{e1} with $k = 1$, and f'_{e2} with $k = 2$, in the first two intrinsic mode functions (IMF), and averaged instantaneous amplitudes of the first two IMFs are used as fault

indicators. The half bandwidth of these local bands in HHT is set as 2 Hz.

The HHT, CHS and the proposed HS technique generate fault indicators from the PSD spectrum. To examine if the fault indicators could be used for different classifiers, both the support vector machine (SVM) [23] and linear discriminant analysis (LDA) [24] are utilized to test the accuracy of different fault detection techniques. A series of tests have been conducted for this verification; however, the test results corresponding to five load conditions (i.e., 0, 20%, 50%, 70% and 100% load levels) will be used for demonstration. In data preparation, 200 data sets are collected for each IM condition (healthy, static air-gap eccentricity fault, and dynamic air-gap eccentricity fault) in each of five load conditions. The sampling frequency is $f_p = 20000$ Hz and the time span of each data set is 3 s. The fault indicators of PSD, HHT, CHS and the proposed HS are extracted from these totally 3000 data sets.

3.2 Experiment Setup

Figure 3 shows the experiment setup used in this test. The tested IMs are 3-phase, 1/3 hp motors made by Marathon Electric. Its speed is controlled by a speed controller (VFD-B) with output frequency 0.1–400 Hz. A magnetic clutch system (PHC-50) is used as the dynamometer to provide external loading, with torque ranging from 1 to 40 N·m. A gearbox (Boston Gear 800) is used to adjust the speed ratio of the dynamometer. An encoder (NSN-1024-2 M-F) is used to measure the shaft speed. Phase current signals are measured by the use of current sensors (LTS 6-NP). A data acquisition board (Quanser Q4) is used for signal measurement. Motor specifications are given in Table 2. The static air-gap eccentricity is implemented by introducing a 0.025 inch horizontal travel of the bearing housing of end bells in the IM. The dynamic air-gap eccentricity is implemented by intentionally bending rotor in the center 0.0127 cm to 0.0254 cm, while making sure the rotor does not bind the stator in the IM [25]. Based on the motor specification, the introduced air-gap eccentricity faults are considered to be at the early stage of the IM fault.

3.3 Static Air-gap Eccentricity Fault Detection

Static air-gap eccentricity fault detection is considered as a binary classification problem; the data sets collected from a healthy IM and an IM with the dynamic air-gap eccentricity defect belong to one class; the data sets collected from the IM with the static air-gap eccentricity defect belong to the other class. The averaged successful rate of ten runs three-fold cross validation in terms of static air-gap eccentricity fault diagnosis using SVM and LDA for classification is summarized in Tables 3 and 4, respectively. It is seen from Tables 3 and 4 that the proposed HS technique has the highest averaged successful rates in both training and testing. The proposed HS technique outperforms PSD under all five load levels, because it could explore more fault information and enhance fault features using HSP. The HS outperforms the CHS in all five scenarios, because the mean value of the local band is a more representative feature for fault detection. HS is superior to the HHT in that more effective fault features are extracted and employed for fault detection.

The score plots of SVM and LDA with respect to the HS static eccentricity fault indicators for static eccentricity diagnosis are illustrated in Figure 4. Totally 600 samples are shown in each plot. The scores of SVM classification and LDA classification are normalized over [–1, 1]. In each axis (x-axis or y-axis), –1 and 1 denote two different classes respectively. The closer the sample is to the –1 or 1, the

Table 5 Averaged successful rates (SR) of ten runs three-fold cross validation in terms of dynamic air-gap eccentricity fault diagnosis using SVM (%)

Load level	0	20	50	70	100
PSD training SR	84.14	63.21	60.68	65.44	61.28
PSD test SR	81.82	60.13	57.11	60.94	58.41
HHT training SR	82.60	64.22	58.73	56.52	60.38
HHT test SR	79.99	60.23	53.67	52.66	59.30
CHS training SR	94.02	91.14	85.97	78.27	75.92
CHS test SR	92.30	88.66	85.71	75.23	74.66
HS training SR	99.47	97.69	98.50	94.74	93.72
HS test SR	98.96	97.13	97.73	94.53	92.47

Table 6 Averaged successful rates (SR) of ten runs three-fold cross validation in terms of dynamic air-gap eccentricity fault diagnosis using LDA (%)

Load level	0	20	50	70	100
PSD training SR	83.95	66.93	67.17	68.22	66.40
PSD test SR	82.73	64.75	65.02	66.87	63.45
HHT training SR	79.40	67.89	67.57	68.24	68.06
HHT test SR	78.75	60.30	65.73	65.42	65.20
CHS training SR	93.51	89.00	89.45	80.79	79.59
CHS test SR	92.88	87.73	88.82	79.67	78.17
HS training SR	99.02	95.99	96.27	94.67	91.78
HS test SR	98.98	95.43	95.47	93.87	91.35

more probably the sample belongs to the class denoted by –1 or 1. The zero-vertical line and zero-horizontal line are the separating hyper-planes to differentiate two classes using SVM and LDA respectively. From Figures 4(a)–4(d), 4(g), and 4(h), it is seen that the two classes could be separated using either SVM or LDA under 0, 20% and 70% load levels. It is seen in Figures 4(e) and 4(f) that there is one sample misclassification in both training and testing in 50% load state. The samples in Figures 4(i) and 4(j) are a bit scattered because heavy load condition weakens fault features, however, the samples could still be correctly classified mostly in 100% load level. Therefore, the proposed HS technique is a useful tool to detect IM static air-gap eccentricity fault in different load conditions.

3.4 Dynamic Air-gap Eccentricity Fault Detection

For dynamic air-gap eccentricity fault diagnosis, the data sets corresponding to healthy IM condition and static air-gap eccentricity condition will belong to one class; the data

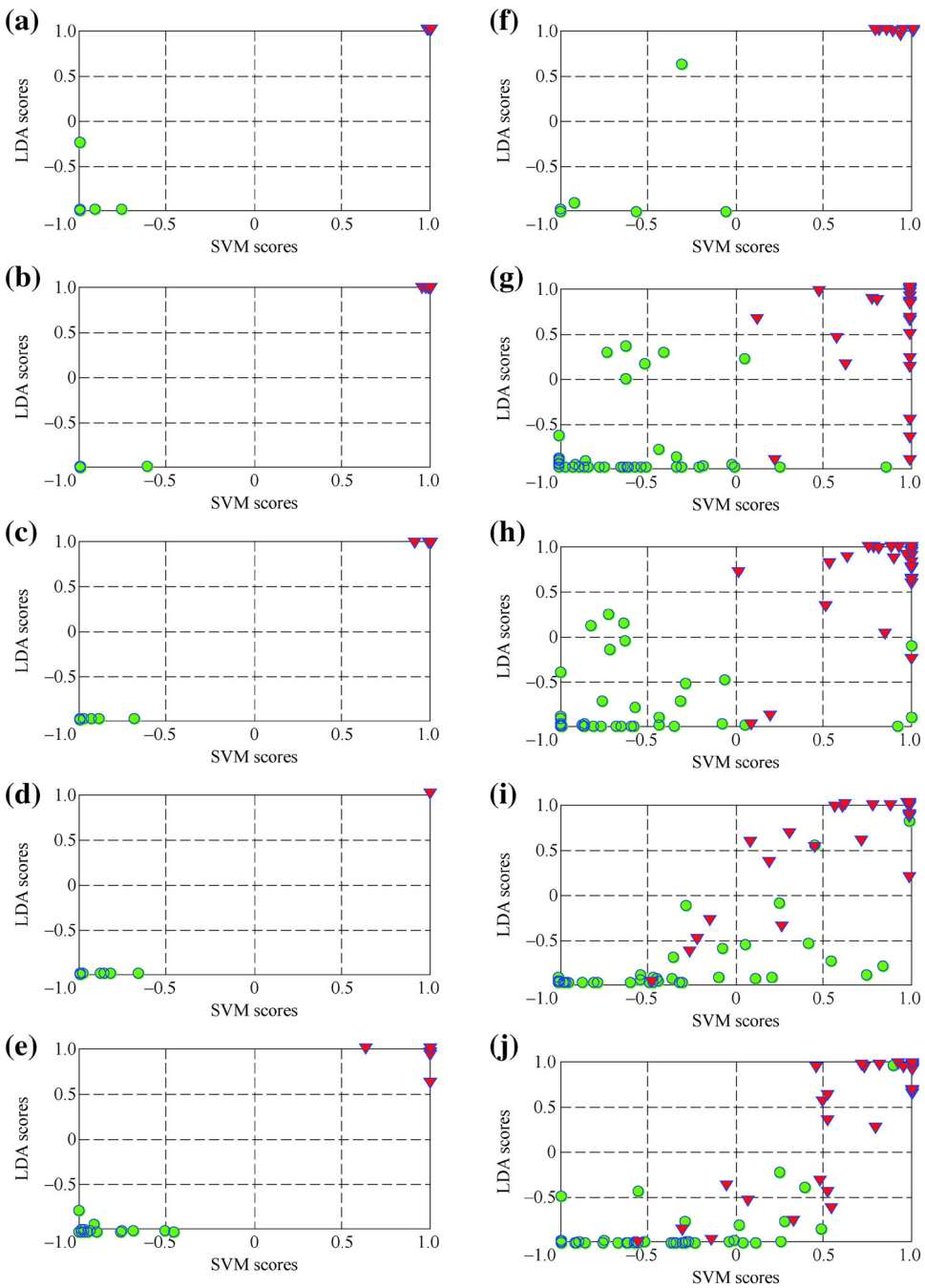

Figure 5 The score plots of SVM and LDA with respect to the HS dynamic eccentricity fault indicators for dynamic eccentricity diagnosis. The training data score distribution with different load conditions: (a) 0%, (c) 20%, (e) 50%, (g) 70% and (i) 100%, and test data score distribution in different conditions: (b) 0%, (d) 20%, (f) 50%, (h) 70% and (j) 100% load conditions. The green circles and the red triangles represent two different class samples respectively

sets corresponding to dynamic air-gap eccentricity condition belong to the other class. The averaged successful rates of ten runs three-fold cross validation in terms of dynamic air-gap eccentricity fault diagnosis using SVM and LDA for classification is given in Tables 5 and 6, respectively. From Tables 5 and 6, it is seen that the proposed HS technique has the highest accuracy in both training and testing. HS technique outperforms PSD in all five scenarios because of the extensive fault information exploration and fault features enhancement. The proposed HS is superior to the CHS in all five cases because of its effective local fault information analysis. HS outperforms HHT because more effective fault features are extracted for fault analysis.

The score plots of SVM and LDA with respect to the HS dynamic eccentricity fault indicators for dynamic eccentricity diagnosis are shown in Figure 5. From Figures 5(a)–5(d), it is seen that the two classes could be separated using either SVM or LDA under 0% and 20% load levels. It can be seen from Figure 5(f) that there is one sample misclassification in testing by LDA in 50% load condition. The samples in Figures 5(g)–5(j) have larger variance due to interference of the heavy load condition; however, most samples could still be correctly classified in 70% and 100% load conditions. It demonstrates that the proposed HS technique is a useful tool to detect IM dynamic air-gap eccentricity fault in different load conditions.

4 Conclusions

A harmonic synthesis (HS) technique is proposed in this work for initial IM air-gap eccentricity fault detection. In the HS, the fault harmonic series are synthesized to enhance fault characteristic features. The local spectra statistical analysis is employed to extract representative features. The SVM classifier and the LDA classifier are utilized to evaluate the performance of different fault detection techniques. The effectiveness of the proposed HS technique is verified by a series of experimental tests under five load conditions: 0%, 20%, 50%, 70% and 100%. Test results show that the proposed HS technique is an effective fault detection tool, and it outperforms the other techniques in all five load conditions. It is able to process massive fault related information, analyze fault features statistically, and enhance representative features for static eccentricity and dynamic eccentricity fault diagnosis based on the current signals. Future research will be undertaken on classification of health state, static eccentricity state and dynamic eccentricity state altogether, as well as the analysis of stochastic resonance based fault detection.

References

1. R Fei, E F Fuchs, H Huag. Comparison of two optimization techniques as applied to three-phase induction motor design. *IEEE Transaction on Energy Conversion*, 1989, 4(4): 651-660.
2. S Nandi, R M Bharadwaj, H A Toliyat. Performance analysis of a three phase induction motor under incipient mixed eccentricity condition. *IEEE Transaction on Energy Conversion*, 2002, 17(3): 392-399.
3. X Li, Q Wu, S Nandi. Performance analysis of a three-phase induction machine with inclined static eccentricity. *IEEE Transactions on Industry Applications*, 2007, 43(2): 531-541.
4. P Zhang, Y Du, T G Habetler, B Lu. A survey of condition monitoring and protection methods for medium-voltage induction motors. *IEEE Transactions on Industry Applications*, 2011, 47(1): 34-46.
5. M E I H Benbouzid. A review of induction motors signature analysis as a medium for faults detection. *IEEE Transactions on Industrial Electronics*, 2000, 47(5): 984-993.
6. J Jung, J Lee, B Kwon. Online diagnosis of induction motors using MCSA. *IEEE Transactions on Industrial Electronics*, 2006, 53(6): 1842-1852.
7. M Blödt, J Regnier, J Faucher. Distinguishing load torque oscillations and eccentricity faults in induction motors using stator current Wigner Distributions. *IEEE Transactions on Industry Applications*, 2009, 45(6): 1991-2000.
8. B Akin, S Choi, U Orguner, H A Toliyat. A simple real-time fault signature monitoring tool for motor-drive-embedded fault diagnosis systems. *IEEE Transactions on Industrial Electronics*, 2011, 58(5): 1990-2001.
9. G Bossio, C D Angelo, J Solsona, V M I García. Application of an additional excitation in inverter-fed induction motors for air-gap eccentricity diagnosis. *IEEE Transaction on Energy Conversion*, 2006, 21(4): 839-847.
10. V Climente-Alarcon, J A Antonino-Daviu, M Riera-Guasp, M Vlcek. Induction motor diagnosis by advanced notch FIR filters and the Wigner – Ville Distribution. *IEEE Transactions on Industrial Electronics*, 2014, 61(8): 4217-4227.
11. J Faiz, M Ojaghi. Instantaneous-power harmonics as indexes for mixed eccentricity fault in mains-fed and squirrel-cage induction motors. *IEEE Transactions on Industrial Electronics*, 2009, 56(11): 4718-4726.
12. X Huang, T G Habetler, R G Harley. Detection of rotor eccentricity faults in a closed-loop drive-connected induction motor using an artificial neural network. *IEEE Transactions on Power Electronics*, 2007, 22(4): 1552-1559.
13. E Esfahani, S Wang, V Sundararajan. Multisensor wireless system for eccentricity and bearing fault detection in induction motors. *IEEE/ASME Transactions on Mechatronics*, 2014, 19(3): 818-826.
14. S Nandi, S Ahmed, H A Toliyat. Detection of rotor slot and other eccentricity related harmonics in a three phase induction motor with different rotor cages. *IEEE Transaction on Energy Conversion*, 2001, 16(3): 253-260.
15. M Riera-Guasp, M Pineda-Sanchez, J Perez-Cruz, et al. Diagnosis of induction motor faults via Gabor analysis of the current

in transient regime. *IEEE Transactions on Instrumentation and Measurement*, 2012, 61(6): 1583-1596.
16. J Park, J Hur. Detection of inter-turn and dynamic eccentricity faults using stator current frequency pattern in IPM-type BLDC motors. *IEEE Transactions on Industrial Electronics*, 2016, 63(3): 1771-1780.
17. S M Mirimani, A Vahedi, F Marignetti, R D Stefano. An online method for static eccentricity fault detection in axial flux machines. *IEEE Transactions on Industrial Electronics*, 2015, 62(3): 1931-1942.
18. P Konar, P Vhattopadhyay. Bearing fault detection of induction motor using wavelet and support vector machines. *Applied Soft Computing*, 2011, 11(6): 4203-4211.
19. A Soualhi, G Clerc, H Razik. Detection and diagnosis of faults in induction motor using an improved artificial ant clustering technique. *IEEE Transactions on Industrial Electronics*, 2013, 60(9): 4053-4062.
20. M Seera, C P Lim. Online motor fault detection and diagnosis using a hybrid FMM-CART model. *IEEE Transactions on Neural Networks and Learning Systems*, 2014, 25(4): 806-812.
21. A M Knight, S P Bertani. Mechanical fault detection in a medium-sized induction motor using stator current monitoring. *IEEE Transaction on Energy Conversion*, 2005, 20(4): 753-760.
22. D G Dorrell, W T Thomson, S Roach. Analysis of airgap flux, current, vibration signals as a function of the combination of static and dynamic airgap eccentricity in 3-phase induction motors. *IEEE Transactions on Industry Applications*, 1997, 33(1): 24-34.
23. N Cristianini, J Shawe-Taylor. *An Introduction to Support Vector Machines and Other Kernel-based Learning Methods*, First Edition, Cambridge: Cambridge University Press, 2000.
24. A J Izenman. *Modern Multivariate Statistical Techniques*, New York: Springer, 2008.
25. Spectra Quest, *User operating manual for machinery fault simulator*. website: www.spectraquest.com.

De Z. Li, received his B.Sc. degree in electrical engineering from *Shandong University, China*, in 2008, M.Sc. degree in control engineering from *Lakehead University, Canada*, in 2010, and PhD degree in mechanical engineering from the *University of Waterloo, Canada*, in 2015. His research interests include machinery health condition monitoring, signal processing, machine learning, mechatronic systems, linear/nonlinear system control and artificial intelligence. E-mail: dli2@lakeheadu.ca.

Wilson Wang, received his M.Eng. in industrial engineering from the *University of Toronto, Toronto, ON, Canada*, in 1998 and the Ph.D. in mechatronics engineering from the *University of Waterloo, Waterloo, ON, Canada*, in 2002. From 2002 to 2004, he was a Senior Scientist with *Mechworks Systems Inc*. He joined the faculty of *Lakehead University, Thunder Bay, ON, Canada*, in 2004, where he is currently a Professor with the *Department of Mechanical Engineering*. His research interests include signal processing, artificial intelligence, machinery condition monitoring, intelligent control, and mechatronics. Tel: +1 (807) 766-7174. E-mail: wwang3@lakeheadu.ca.

Fathy Ismail, received the B.Sc. and M.Sc. degrees in mechanical and production engineering, in 1970 and 1974, respectively, from *Alexandria University, Egypt*, and the Ph.D. degree from *McMaster University, Hamilton, Ontario, Canada*, in 1983. He joined the *University of Waterloo, Waterloo, Ontario, Canada*, in 1983, and is currently a professor in the *Department of Mechanical and Mechatronics Engineering*. He has served as the chair of the department and the associate dean of the faculty of engineering for graduate studies. His research interests include machining dynamics, high-speed machining, modeling structures from modal analysis testing, and machinery health condition monitoring and diagnosis. E-mail: fmismail@uwaterloo.ca.